DTU Library

Theory of Al2O3 incorporation in SiO2

Lægsgaard, Jesper

Theory of Al$_2$O$_3$ incorporation in SiO$_2$

J. Lægsgaard

Research Center COM, Technical University of Denmark, Bldg. 345v, DK-2800 Lyngby, Denmark
(Received 12 November 2001; published 19 April 2002)

Different possible forms of Al$_2$O$_3$ units in a SiO$_2$ network are studied theoretically within the framework of density-functional theory. Total-energy differences between the various configurations are obtained, and simple thermodynamical arguments are used to provide an estimate of their relative importance at different Al concentrations. Some experimentally accessible quantities (hyperfine parameters, electric-field gradient tensors, and core-level chemical shifts) are derived, and compared with experimental data where available. The results show that Al ions at low Al$_2$O$_3$ concentrations will be present as isolated impurities bound to three or four O atoms, whereas at higher concentrations clusters consisting of four Al ions will form. In these clusters both four- and five-coordinated Al can occur, but no energetic preference for the five-coordinated state is found.

I. INTRODUCTION

The properties of Al impurities in silica glass have in recent years become an important topic due to the commercial use of rare-earth doped silica glass for creating active (i.e., light-amplifying) devices used for optical communications systems. Al codoping plays a crucial role in the fabrication of components with useful gain coefficients as it has been found to prevent the clustering of rare-earth dopants which would otherwise strongly reduce the attainable population inversion for high rare-earth concentrations.[1,2] No microscopic model for the interactions between rare earths and Al exist at the moment, and even the behavior of Al impurities in the absence of rare-earth elements is poorly understood. Previous experimental work on crystalline quartz as well as various forms of silicate glasses has indicated that Al is present in a number of different states depending on the concentration of Al and other impurities in the material. Extensive electron paramagnetic resonance (EPR) studies have established that Al in natural quartz is predominantly incorporated in Si-substitutional positions with the missing electron provided by a nearby alkali element (such as H, Li, Na, etc.).[3–7] Also Al ions implanted in silica were found to occupy substitutional positions, pushing Si atoms into the interstitial region.[8–11] However, the state of fully oxidized Al impurities (that is, Al$_2$O$_3$ units) in a silica network free of other impurities is still an open question. Brower[12,13] found EPR evidence of three-coordinated Al ions in silica fused from natural quartz with low alkali content, but a recent EXAFS[14] study of glass with an Al$_2$O$_3$ concentration of ~0.4 mole % (compared to the ~10–100 ppm weight Al concentration in natural quartz) found only evidence of four-coordinated Al species. NMR studies at still higher (>1 mole %) concentrations resolve signals from both four-, five-, and six-coordinated Al (the assignment of the five-coordinated signal is somewhat controversial).[15–19]

A number of theoretical investigations of Al impurities in silica have appeared over the years, most of them being concerned with the structure and hyperfine parameters of Si-substitutional Al with or without compensating ions.[20–26] Such calculations have played an important role in establishing the structural models for compensated substitutional Al

impurities. In addition, small molecules and zeolite structures containing oxidized Si and Al ions have been studied, primarily with the purpose of extracting electric-field gradients (EFG's) at Si, Al, and O nuclei.[27,28]

The purpose of the present work is to shed light on the behavior of Al in lightly doped ($\lesssim$1 mole % Al$_2$O$_3$) SiO$_2$ by means of parameter-free density-functional theory (DFT). To this end, some simple structural models for Al$_2$O$_3$ units in a SiO$_2$ matrix are investigated. The quantities of interest are total energies and geometric structures, hyperfine coupling constants, core-level shifts, and electric-field gradients. Simple thermodynamic models based on the total-energy results serve to give a feel for the magnitude of entropy effects. The calculations are done in repeated-cell geometries based on crystalline quartz forms. The possibility of generalizing the results to the important case of amorphous silica is carefully discussed, although no attempt at a direct simulation of the amorphous environment is made. On the basis of the theoretical findings various experimental results are analyzed and discussed.

The rest of the paper is organized as follows: In Sec. II the theoretical approach is outlined. This includes both the structural models considered, and the calculational techniques employed. In Sec. III the results of the DFT calculations and some thermodynamical model calculations are presented. In Sec. IV these results together with experimental information are used as a basis for discussing various models for the behavior of Al impurities in silica glass. Section V summarizes the results and conclusions.

II. THEORETICAL APPROACH

A. Structural models for Al$_2$O$_3$ in silica

The investigation of impurity behavior in silica materials is greatly complicated by the fact that even the energy landscape for pure silica has a multitude of local minima. This is evidenced by the existence of 19 crystalline silica allotropes and also by the ease with which amorphous silica is formed. Further complications are, of course, introduced by the addition of other chemical species than the network constituents, and an exhaustive exploration of the local energy minima exhibited by a reasonably sized piece of impurity-containing

silica using accurate quantum-mechanical methods at the moment appears computationally prohibitive.

The complexity of the energy landscape may be greatly reduced by assuming a crystalline host material and neglecting the possibility of network topology reconstructions around the impurities. This approach is supported by the observation that the local chemical environment around a particular atom (which experimentally can be probed through neutron scattering or x-ray diffraction) in amorphous silica is similar to that in the crystalline forms. The disorder comes about through a loss of intermediate- and long-range order. Therefore local impurity chemistry should not differ too much between crystalline and amorphous silica, and the use of crystalline impurity hosts in theoretical studies has considerable merit in predicting local observables such as hyperfine parameters and core-level shifts even for the amorphous case. This strategy is also adopted in the present work, using in most cases crystalline α-quartz as the host material. However, it is important to keep in mind that the results obtained are, in principle, specific for the chosen crystal form, and that their validity further depends on the assumption that no reconstructions of the network topology takes place.

Due to the high degree of local chemical order in silica, the nearest-neighbor shell of a given atom can be unambiguously identified, even in the impurity geometries to be considered in this paper. Therefore the concept of coordination number (or number of atoms in the nearest-neighbor shell) of a given atom is well defined. In the following, $X[n]$ will denote an atom of type X with n nearest neighbors. For instance, $Al[4]$ denotes an Al atom bonded to four O atoms, whereas $O[2]$ denotes an O atom bonded to two Si/Al atoms.

Even with the above-mentioned restrictions a number of Al impurity states can be imagined, depending on the number of Al atoms present. In the following only the simplest and most obvious configurations will be considered. Introduction of an Al_2O_3 unit in a SiO_2 network can be regarded as the introduction of two AlO_2 groups (e.g., two Si-substitutional Al atoms) along with an O vacancy (hereafter denoted V_O). If these "elementary particles" are assumed to be widely separated this implies either a corresponding charge separation (each substitutional Al carrying a negative charge taken from the O vacancy), or the existence of unpaired spins at the Al ions. Since the well-established EPR signal from neutral substitutional Al is not observed in unirradiated Al-containing silica, it follows that charge separation must occur if this Al_2O_3 state is present. Total-energy calculations for charged impurities with periodic boundary conditions (which, as explained in the next subsection, are adopted here) are a nontrivial matter and therefore these states will not be considered here. The need for charge separation is reduced if the O vacancy binds to one of the Al atoms, and eliminated if it binds to both. I shall denote these structures AlV_O and Al_2V_O, respectively. They are schematically depicted in Figs. 1(a), 1(b). The $Si[3]$ and $Al[3]$ atoms constitute electron traps due to the presence of dangling sp^3 orbitals. The AlV_O state [Fig. 1(a)] is a deep trap, since the paramagnetic configuration is the neutral one, whereas the Al_2V_O state is a shallow trap, since the paramagnetic state is negatively charged. In the following, the para-
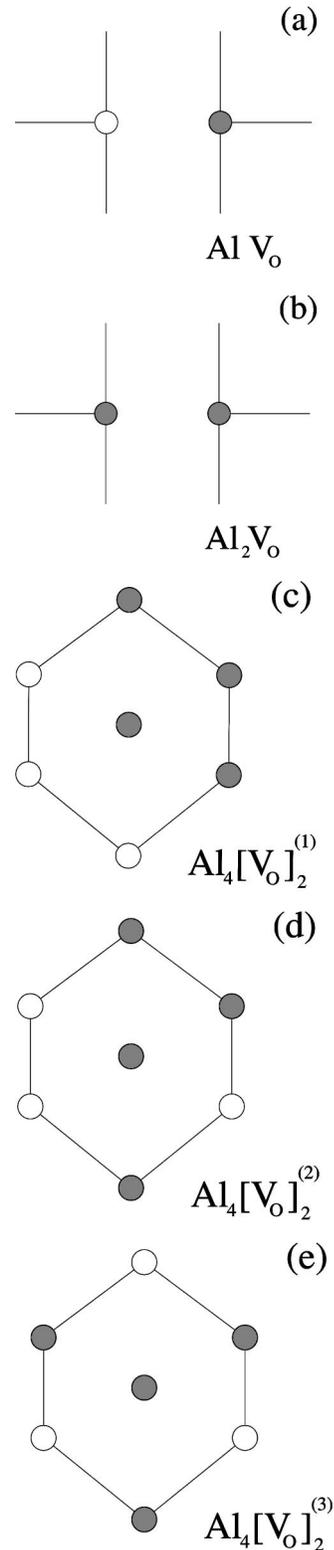

FIG. 1. Pictorial representations of the impurity states investigated. The white circles represent Si cations while the shaded circles represent Al. The links between cations (drawn as straight lines) proceed via two-coordinated O ligands which are not shown explicitly.

magnetic states of AlV_O and Al$_2$$V_O$ will be studied with the purpose of extracting EPR parameters.

In the unrelaxed α-quartz structure each Al ion in the Al$_2$$V_O$ state is threefold coordinated, and the state is neutral and nonmagnetic. However, although the dangling Al sp^3 orbitals are unoccupied, they may still be chemically active, due to the presence of nonbonding $2p$ orbitals on the O atoms in the silica network. Although the O $2p$ levels are considerably lower in energy, the electrons in these levels may gain some hybridization energy by bonding to the empty Al sp^3 orbital. This would lead to the formation of an Al[4] and an O[3] atom in the lattice. This idea, commonly known as the "tricluster" hypothesis, was originally put forward by Lacy.[29] A similar rebonding mechanism at positively charged O vacancies is thought to be the origin of the paramagnetic E_1' center in α-quartz.[30] However, the formation of the extra bond will require a distortion of the silica network with an elastic energy penalty whose magnitude will depend on the local environment.

Another structural model which has been suggested by several authors is the formation of three Si-substitutional Al ions compensated by a fourth Al^{3+} ion residing in the interstitial parts of the silica network.[31–33] Since each substitutional Al ion needs an extra electron (from the interstitial Al^{3+}) to fill all bonds, it is clear that there will be a strong electrostatic attraction between substitutional and interstitial ions. In fact, the energy gained by moving all four constituent ions together can be estimated as

$$\Delta E = \frac{6e^2}{\epsilon d}, \tag{1}$$

where ϵ is the dielectric constant of silica and d is the distance between the Al ions. Taking $d = 3$ Å (approximately the shortest distance between Si atoms in silica) and $\epsilon = 4.48$,[34] one obtains $\Delta E = 6.43$ eV, so in the present work I will only consider the case where the interstitial Al^{3+} ion resides next to the substitutional Al's, a structure I shall denote as Al$_4$[V_O]$_2$. Even with this restriction it is clear that there is a large number of possible variations to this structural theme, of which I will only investigate a few examples. A common feature of crystalline silica allotropes is the appearance of ring structures containing six silicon atoms, and these rings are also thought to be abundant in amorphous silica. I will therefore investigate some Al$_4$[V_O]$_2$ structures in which the substitutional Al atoms are all present in one six-member ring. Three cases, schematically depicted in Figs. 1(c)–(e), are considered: One [Fig. 1(c)] in which all Al atoms has at least one Al neighbor in the ring, one [Fig. 1(d)] in which two Al atoms are neighbors, and finally [Fig. 1(e)] one in which the Al atoms are evenly distributed over the ring. In the following, these states will be denoted Al$_4$[V_O]$_2^{(1)}$, Al$_4$[V_O]$_2^{(2)}$, and Al$_4$[V_O]$_2^{(3)}$, respectively.

B. Computational methods

The study of the Al configurations outlined in the previous subsection is performed within the framework of density-functional theory (DFT).[35,36] The exchange-correlation energy is described in the approximation proposed by Perdew and Wang (PW91),[37] and the resulting Kohn-Sham equations are solved in a plane-wave representation using Vanderbilt's ultrasoft pseudopotential (US-PP) scheme.[38,39] Unless otherwise stated, the plane-wave expansion of the wave functions is cut off at a kinetic energy of 25 Ry, and Brillouin-zone integrations are approximated by sampling only the Γ point. In most cases, the Al impurities are immersed in an α-quartz host, which is the stable crystalline form of silica at low temperatures. In addition, a few calculations have been made using α-cristobalite as a host material. All calculations in the α-quartz host are done in a supercell consisting of eight elementary unit cells or 24 SiO$_2$ formula units, whereas in the case of α-cristobalite a supercell of four elementary unit cells (16 formula units) is used. For α-quartz, lattice parameters were fixed at the theoretical equilibrium values for pure silica as calculated within the present approach ($a = 5.05$ Å, $c/a = 1.097$). The α-cristobalite calculations were done at the experimental lattice constants. Full structural optimizations were performed using a conjugate-gradient algorithm searching for the nearest local minimum in configuration space. Relaxations were performed until the length of the total force vector was less than 0.15 eV/Å, except for the AlV_O states which are only studied to extract EPR properties.

From the total-energy results obtained in the supercell calculations impurity state formation energies can be obtained from the formula

$$\begin{aligned} E_i^{form} = E_h[x_{ih}\text{SiO}_2 : y_i\text{Al}_2\text{O}_3] \\ - x_{ih}E_h[\text{SiO}_2] - y_i(2E_{at}[\text{Al}] + 3E_{at}[\text{O}]). \end{aligned} \tag{2}$$

Here i indexes the various impurity states (Al$_2$$V_O$, Al$_4$[$V_O$]$_2^{(1)}$, etc.), while h indexes the crystalline hosts (α-quartz and α-cristobalite). x_{ih}, y_i are the number of SiO$_2$ and Al$_2$O$_3$ units in the supercell, e.g., for Al$_2$$V_O$ in cristobalite $x = 14$ and $y = 1$, while for Al$_4$[V_O]$_2$ in α-quartz $x = 21$, $y = 2$. $E_h[\text{SiO}_2]$ denotes the energy per formula unit of a pure SiO$_2$ supercell calculated with same parameters for lattice constants, plane-wave cutoff, **k**-point sampling, etc. $E_{at}[\text{Al}], E_{at}[\text{O}]$ is the energy of free Al,O atoms. The choice of reference state is of no consequence in the present paper since only formation energy differences will be relevant (it is not my intention to model the glass formation process). The computation of absolute formation energies, whether using free-atom or crystalline reference energies, is prone to errors from basis-set cutoff, **k**-point sampling and the finite size of the supercell. However, in the formation energy differences these errors cancel to a large extent.

The calculation of hyperfine parameters and electric-field gradient tensors require knowledge of the wave function close to, or even right at, the nucleus, which appears to present a problem, as the pseudopotentials do not describe the wave function correctly in this region of space. To overcome this problem, I reconstruct the true wave function in the core region by augmenting the pseudo wave function along the lines described in Ref. 40. Using this procedure, one obtains a wave function very similar to that of the

projector-augmented wave (PAW) scheme introduced by Blöchl,[41,42] which has been shown to give rather accurate results for the properties of interest here.[43–45] The Al ultrasoft pseudopotential used throughout has two projector functions in the s channel and one in the p and d channels. For the isotropic part of the hyperfine tensor, core-polarization effects are approximately taken into account by recalculating the core states while keeping the spin-polarized valence electron density fixed. This is not an exact approach, as it ignores the back reaction of the core spin polarization on the valence electron density, but it serves to give an idea of the magnitude of the core-polarization effect. In the present case, core-polarization was found to affect the isotropic hyperfine parameters by about 1% in all calculations.

To estimate Al core-level shifts new Al pseudopotentials with a hole present in either the $1s$ or $2p$ channel were constructed. One Al atom in the supercell is then described by such a potential while the total-number of electrons is kept equal to that of the neutral cell without core holes. The total-energy difference between $1s$ and $2p$ hole states provides a measure of the core-valence interaction contribution to the K_α transition energy, and can thereby be used to deduce chemical shifts. It has recently been demonstrated that this approach is able to predict chemical shifts of Al, Si, and Ge lines in various oxide compounds to an accuracy of 10% or better,[11] and it therefore appears suitable for predicting line positions in the present problem. In the same way, the total-energy difference between states with a $1s$ (or $2p$) hole in different positions provides a measure of the chemical shift of this core level between the two Al atoms in question. No attempt at calculating absolute transition energies is made. Core-level shifts of O $1s$ levels are calculated in a similar way, introducing an O pseudopotential with a hole in the $1s$ shell at the O atoms of interest while keeping the number of valence electrons fixed. By comparing total-energy values with the $1s$ hole in different positions core-level shifts between "ordinary" silica O atoms and those in the vicinity of the Al impurities can be deduced.

The treatment of charged states in a supercell approach is a delicate problem, since the long range of the Coulomb potential leads to a divergency in the electrostatic energy when the charged impurity is periodically repeated. For the treatment of the $[\mathrm{Al}_2 V_O]^-$ state, I shall adopt the common solution of adding a uniform background charge to eliminate the divergency. This implies a substantial error in the total energy, and possibly also minor errors in the equilibrium structures. However, for estimating the magnitudes of hyperfine coupling constants, which is the main reason for including this state here, the approach should be acceptable.

III. NUMERICAL RESULTS

A. Geometries and electronic structures

1. AlV_O

The neutral AlV_O state has an unpaired spin, and therefore cannot exist in appreciable quantities in ordinary silica, as its EPR activity would otherwise have been noticed. The reason for including it in the present study is to investigate its EPR properties. If charged AlV_O units exist in the normal state of silica it should be possible to observe the EPR signals from neutral AlV_O states induced upon irradiation of the material. Since accurate total-energy data are not required for this Al state the structural relaxations have not been performed as thoroughly as for the other states studied. Relaxations have been terminated when the length of the total force vector was below 0.3 eV/Å, and have mostly been performed without spin polarization.

The O vacancy in pure silica has been the subject of several theoretical studies in recent years.[46,30,45] It has been found that the neutral O vacancy in α-quartz has one stable geometry where the dangling orbitals on the Si atoms hybridize to each other, and the distance between the two Si atoms sharing the vacancy becomes around 2.4–2.5 Å. The positively charged O vacancy, on the other hand, has two metastable minima separated by an energy barrier. One minimum is similar to the neutral structure, with only one electron in the Si-Si bond, which expands to about 3 Å. In the other, this electron localizes on one Si atom, whereas the second Si atom is displaced and its dangling orbital rebonds with the nonbonding $2p$ state of a neighboring O atom. In the α-quartz structure, the two Si atoms sharing an O vacancy are not equivalent since the bond lengths to the O atom that was removed are slightly different. Only the long-bonded Si atom has a stable rebonded configuration. This configuraion is commonly known as the silica E_1' center. Concerning the relative stability of the two states somewhat different results have been found using different theoretical approaches. Using the PAW technique and a generalized gradient approximation (GGA) energy functional Blöchl found that the two states were almost degenerate with an energy difference of only 0.04 eV (the rebonded state having the lower energy), Boero *et al.* reported a 0.3-eV difference from US-PP calculations within the local-density approximation (LDA), whereas the Hartree-Fock cluster calculations of Pacchioni and Ieranò yielded an energy difference of 0.64 eV.[46]

When one of the cations sharing the O vacancy is an Al atom, the electronic structure of the neutral defect is similar to that of the positively charged O vacancy in pure silica, since Al has one valence electron less than Si. Therefore one may expect that also the energy landscape of the neutral AlV_O state will resemble that of the positively charged α-quartz O vacancy. I have used the equilibrium geometries for the pure-silica vacancy as starting points for the structural relaxations of the AlV_O states, substituting one of the Si cations with Al. Since in each of the two stable geometries of the charged Si-Si vacancy there are two inequivalent Si cations to substitute there are in principle four possible states to consider. In two of them, both the Si and Al cations will bond to only three O atoms. Since the hyperfine parameters for Si and Al must be expected to be very similar (except for the directionality of the anisotropic tensor) in these two cases only one (with Al at the short-bonded site) will be treated here. On the other hand, when one of the cations is rebonded, it is important for the spin distribution, and therefore the hyperfine parameters, whether the rebonded cation is Si or Al. Therefore both these cases have been investigated. All the relaxed AlV_O geometries are shown in Fig. 2, with bond
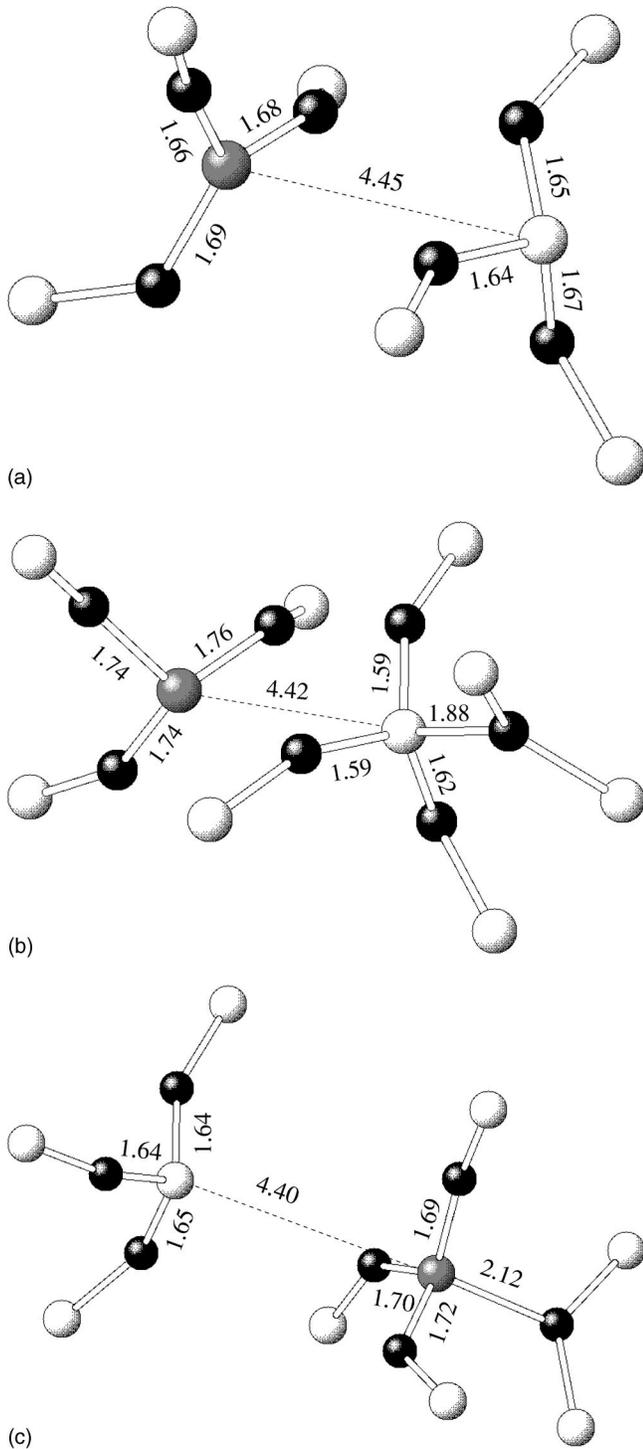
FIG. 2. Relaxed geometries of the various AlV$_O$ states considered. White spheres are Si atoms, gray spheres Al, and black spheres O. (a) Al[3],Si[3] with Al on the short-bonded side of the O vacancy. (b) Al[3],Si[4], cation sites as in (a). (c) Si[3],Al[4] with cation sites interchanged relative to (a) and (b). Some bond lengths are given in Å.

lengths in Å. Judging from the spin-density distribution and in particular the hyperfine parameters (to be discussed in Sec. III C), the unpaired electron does not localize strongly on the Al cation in any of the structures considered. In fact, in the

nonrebonded geometry the electron is almost completely localized on Si, and the distance between the cations is ~4.45 Å, suggesting that Si-Al hybridization does not play an appreciable role in determining the structure. This is in contrast to the situation at a Si-Si vacancy, where the Si-Si distance in the positive charge state is about 3 Å and appreciable Si-Si hybridization remains. The highest spin density on the Al site is found for the state in Fig. 2(b) with rebonded Si, as expected. In this state, the unpaired spin is rather delocalized, with appreciable weigth on both Al, Si, and in the interstitial region.

The tendency of the unpaired electron to localize on Si rather than Al is a consequence of the fact that the sp levels on Si are lower in energy than those on Al. The total energies for the various AlV$_O$ states also reflect this fact: The state in Fig. 2(c) with rebonded Al is about 1.3 eV lower in energy than that with rebonded Si [Fig. 2(b)], and ~0.5 eV lower than the state without rebonding. This is because a structure with the unpaired spin present in the low-energy Si sp orbitals is preferred. The energy of the structure in Fig. 2(c) is then further lowered compared to that of Fig. 2(a) by the formation of an extra Al-O bond. It is interesting to note, however, that this bond is weaker (judging from the bond length) than the corresponding Si-O bond in Fig. 2(b). This suggests that, if the unpaired spin is removed, so that a positively charged AlV$_O$ state is formed, it will be favorable to have Si rather than Al at the rebonded site. Therefore if neutral AlV$_O$ states observed in irradiated samples are assumed to be formed from positively charged precursors it is possible that the state in Fig. 2(b) will be present, although metastable, in spite of its higher energy.

2. Al$_2$V$_O$ and [Al$_2$V$_O$]$^-$

When two Al atoms share an O vacancy the electronic structure is similar to that of a doubly charged O vacancy in pure silica. Since no electrons need to be accommodated in the dangling cation orbitals, one would *a priori* expect both Al atoms to rebond in the manner discussed in the previous section. Indeed, it is found that the nonrebonded energy minimum goes away, but I have not been able to find any stable configuration in which the short-bonded Al atom forms an additional bond. Thus, as can be seen from Fig. 3(a), in the equilibrium geometry there is one Al[3] atom and one Al[4] with a somewhat stretched fourth bond. This finding is very important, since it shows that the rebonding happens at the expense of lattice distortion energy, and therefore is dependent on a favorable local environment. The Al-Al distance in the relaxed state is 4.82 Å, suggesting that no chemical interaction between the Al ions is present. This would indeed be unexpected given that both the dangling Al orbitals are empty. The implications of these results for the possible states of Al in amorphous silica will be discussed below.

In order to investigate the dependence of the rebonding mechanism on the local environment, the Al$_2$V$_O$ configuration was also studied within an α-cristobalite host, as described in Sec. II B. In contrast to the case of α-quartz two local minima were found in the α-cristobalite host, one similar to the rebonded state in α-quartz, with a bond length of
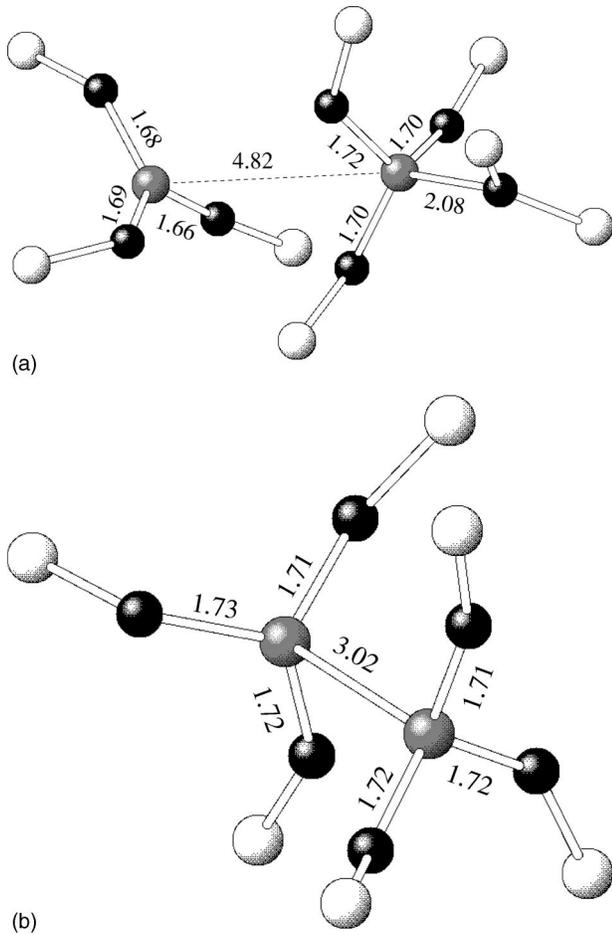
FIG. 3. Relaxed geometries of the Al_2V_O (a) and $[Al_2V_O]^-$ (b) states. Symbols and units as in Fig. 2.

2.05 Å for the extra Al-O bond, and another metastable state in which this distance had expanded to 2.75 Å, so that both Al ions could be considered to be in the Al[3] state.

The dangling orbital on the Al[3] atom constitute a localized state in the silica band gap and can as such act as an electron trap. EPR evidence of such trapped electrons was reported by Brower.[12,13] To investigate the EPR properties of this trap I have performed DFT calculations for the negatively charged Al_2V_O state, $[Al_2V_O]^-$, in the α-quartz host. If the electron is added to the neutral equilibrium geometry without structural relaxation it is indeed found to localize on the Al[3] atom. This structure is not stable, but relaxes into a state in which the Al ions bond to each other, and the unpaired spin is evenly distributed over both Al sites. The equilibrium geometry is shown in Fig. 3(b). The Al-Al distance of 3.02 Å is similar to what was found for the Si-Si bond length at a positively charged O vacancy in pure silica by Blöchl.

3. $Al_4[V_O]_2$

When the $Al_4[V_O]_2$ structures schematically shown in Fig. 1(b) are released they all stabilize in geometries where the Al ions initially substituting for Si in the silica network stay four coordinated although with some degree of disper-

sion in the bond lengths. The behavior of the interstitial Al ion is state dependent. In the $Al_4[V_O]_2^{(1)}$ and $Al_4[V_O]_2^{(3)}$ geometries, the interstitial Al relaxes into a five-coordinated position, whereas in the $Al_4[V_O]_2^{(2)}$ state it ends up being four coordinated, with bond lengths similar to the substitutional Al ions. The geometries are shown in Fig. 4. For the sake of clarity, only the atoms in the Al-containing six-member ring, the interstitial Al and its nearest neighbors have been included. It should be noted that all the O atoms bonded to the interstitial Al are three coordinated although some of them do not appear as such in the figure because they are bonded to Si atoms outside the ring. The mean and variance of the bond lengths for the first and second coordination shells are given in Table I along with the extended x-ray-absorption fine-structure (EXAFS) results recently reported by Sen.[14] The agreement between theory and experiment is quite good, especially for the bond lengths. In the second neighbor shell both coordination numbers and the mean-square deviation of the bond lengths are somewhat overestimated by the theory. In this connection it should be noted that these parameters are correlated in the EXAFS data analysis, and can be increased/decreased simultaneously over some finite range without compromising the quality of the fit to the raw data (Sen estimates an uncertainty of ± 1 for the coordination number). However, from the total-energy results to be presented in the next subsection it can be seen that low bond length dispersion seems to correlate with low total energy. It is therefore to be expected that the present supercell model, with its limited degrees of freedom for structural relaxation, will overestimate the bond length dispersion in an amorphous silica network. On the other hand, the second-shell coordination number is more or less dictated by the structural model: The substitutional Al ions have four Si/Al second-nearest neighbors in the silica network and are, in addition, close to the interstitial Al giving a second-shell coordination of 5. Only in the second shell of the interstitial ion some variations in coordination number between different structures is seen.

Considering the nature of the O linkages it is interesting to notice that no O[2] species bonded to two Al ions (Al-O-Al links) are found, in spite of the proximity of the four Al ions. Most of the O[3] species are bonded to two Al and one Si atom, however, O atoms with three Al neighbors are found in the $Al_4[V_O]_2^{(1)}$ and $Al_4[V_O]_2^{(2)}$ structures and one O[3] atom with two Si neighbors is found in $Al_4[V_O]_2^{(2)}$.

B. Total energies and thermodynamics

The formation energies calculated for the various Al_2O_3 geometries are given in Table II. All energies are per Al_2O_3 unit and are measured relative to the $Al_4[V_O]_2^{(2)}$ state, which is lowest in energy. Considering first the results obtained in the α-quartz supercell, the $Al_4[V_O]_2^{(2)}$ and $Al_4[V_O]_2^{(3)}$ states are seen to be nearly degenerate in energy, while the $Al_4[V_O]_2^{(1)}$ is slightly less favorable. However, all $Al_4[V_O]_2$ configurations are clearly favored over the Al_2V_O state. This is no surprise, given that there are $\sim$ eight Al-O bonds per Al_2O_3 unit in the $Al_4[V_O]_2$ states compared to seven in the Al_2V_O geometry, and that one of the bonds in the latter is
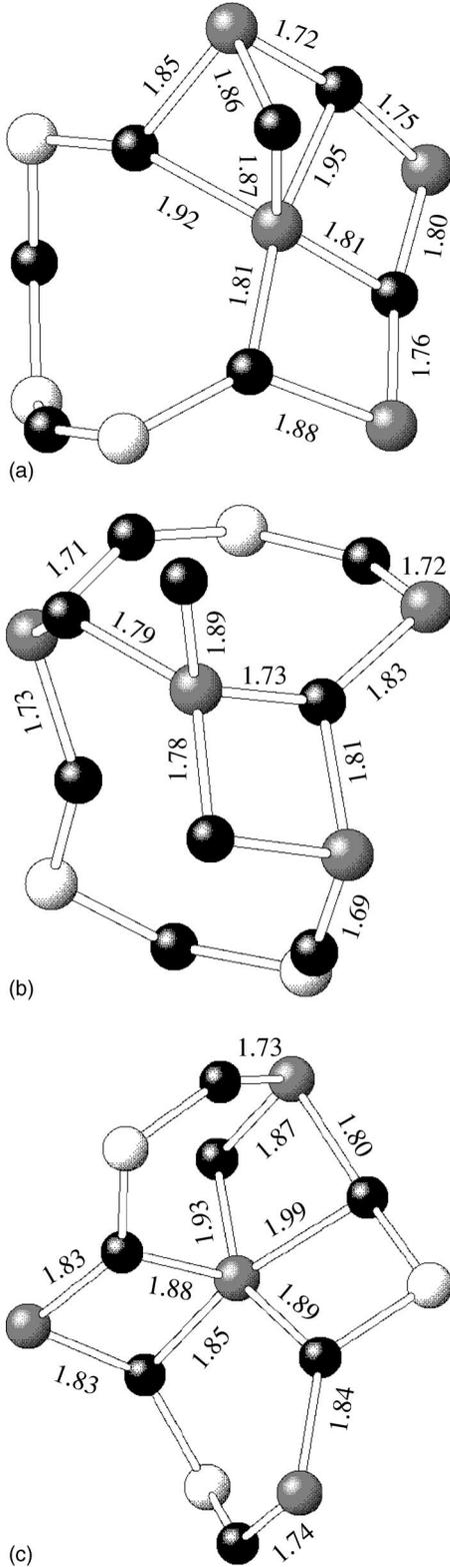
FIG. 4. Relaxed geometries of the $Al_4[V_O]_2^{(1)}$ (a), $Al_4[V_O]_2^{(2)}$ (b), and $Al_4[V_O]_2^{(3)}$ (c) states. Symbols and units as in Figs. 2 and 3.

weak. The energy gained from forming the seventh Al-O bond in Al_2V_O can be estimated from the results obtained in the α-cristobalite structure, where two local minima were found, one of which (denoted $Al_2V_O^{(2)}$ in Table I) practically

TABLE I. Local structural parameters averaged over the Al ions in the various $Al_4[V_O]_2$ impurity states considered. Coordination numbers (Z), bond lengths (d), and mean-square deviation of bond lengths (σ^2) are given for the first and second neighbor shell (consisting, respectively, of O and Si/Al atoms). Units are Å and Å^2.

System	Z_1	d_1	σ_1^2	Z_2	d_2	σ_2^2
$Al_4[V_O]_2^{(1)}$	4.25	1.79	0.007	5.25	3.06	0.127
$Al_4[V_O]_2^{(2)}$	4	1.77	0.006	5.25	3.11	0.048
$Al_4[V_O]_2^{(3)}$	4.25	1.80	0.008	5.5	3.08	0.057
Expt. (Ref. 14)	4	1.77	0.004	4	3.12	0.024

has two Al[3] ions. In the cristobalite structure the gain is only 0.1 eV, whereas the formation energy of Al_2V_O in α-quartz is 0.44 eV lower than that of the metastable Al_2V_O state in the cristobalite host. Since the length of the stretched bond is similar in the two hosts (the seventh bond in cristobalite is actually slightly shorter than that in α-quartz) it is clear that differences in the elastic energy cost of lattice deformation plays a considerable role in determining these energy gains. In the present case, the energy difference between the different hosts may, at least in part, be caused by the fact that the supercell used is larger for α-quartz than for α-cristobalite, thus providing more degrees of freedom for the structural relaxations.

Since the formation of $Al_4[V_O]_2$ structures requires two Al_2O_3 units, the Al_2V_O state, although disfavored from total-energy considerations alone, will be favored by entropy effects. A full simulation of finite-temperature equilibrium thermodynamics is beyond the scope of the present work, and might not even be relevant for all types of glass. However, it is interesting to consider a few simplified thermodynamical models in order to shed light on the implications of the total-energy results quoted above. It should, of course, be stressed that the results obtained for impurity state concentrations are order-of-magnitude estimates rather than accurate quantitative predictions.

Considering the Al_2O_3 units to be moving in a fully polymerized silica network the transformation between the two main impurity models investigated here can be written as the reaction

$$2Al_2V_O \rightleftharpoons Al_4[V_O]_2. \qquad (3)$$
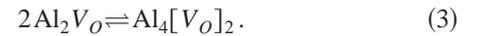
TABLE II. Formation energies (relative to the $Al_4[V_O]_2^{(2)}$ state) for the various Al impurity states considered here, as calculated from Eq. (2).

System	Host	E^{form}/Al_2O_3 (eV)
Al_2V_O	α-quartz	1.40
$Al_2V_O^{(1)}$	α-crist.	1.73
$Al_2V_O^{(2)}$	α-crist.	1.84
$Al_4[V_O]_2^{(1)}$	α-quartz	0.23
$Al_4[V_O]_2^{(2)}$	α-quartz	0
$Al_4[V_O]_2^{(3)}$	α-quartz	0.04

Neglecting the contributions from vibrational entropy and impurity interactions, the Helmholz free energy of the impurities may be written in the form

$$F = \sum_i F_i, \tag{4}$$

$$F_i = -kTN_i(\ln \zeta_i - \ln N_i + 1), \tag{5}$$

$$\zeta_i = \sum_s \exp\left(-\frac{\varepsilon(s)}{kT}\right). \tag{6}$$

Here i indexes the Al complexes Al_2V_O, $Al_4[V_O]_2$, s denotes the various possible states of a given complex, and $\varepsilon(s)$ denotes the energy of state s. From this expression one can derive the law of mass action

$$\frac{N_{Al_4[V_O]_2}}{N^2_{Al_2V_O}} = \frac{\zeta_{Al_4[V_O]_2}}{\zeta^2_{Al_2V_O}}. \tag{7}$$

The state sums in the ζ parameters should now include all possible states of a given composition. For the Al_2V_O "molecule" there is obviously one possible state for each O site in the lattice, so that

$$\zeta_{Al_2V_O} = 2N_{lat}\exp\left(-\frac{\varepsilon(Al_2V_O)}{kT}\right), \tag{8}$$

where N_{lat} is the number of cation sites in the lattice (i.e., in the limit of low Al concentration $N_{lat} \approx N_{Si}$). For the various $Al_4[V_O]_2$ states I shall assume that all structures having the schematic form depicted in Fig. 1(b) are degenerate, and similar for the structures in Figs. 1(c) and 1(d). Only these $Al_4[V_O]_2$ geometries will be included in the calculation. This is obviously an oversimplification and probably means that the results provide a lower bound on the $Al_4[V_O]_2$ abundance since not all relevant $Al_4[V_O]_2$ geometries are taken into account. In α-quartz there is one six-member ring per cation site, so the expression for $\zeta_{Al_4[V_O]_2}$ now becomes

$$\zeta_{Al_4[V_O]_2} = N_{lat}\sum_{i=1}^{3} x_i\exp\left(\frac{-\varepsilon(Al_4[V_O]_2)^{(i)}}{kT}\right) \tag{9}$$

with $x_1 = 6$, $x_2 = 12$, $x_3 = 2$. Equation (7) may then be cast in the form

$$\frac{c_{Al_4[V_O]_2}}{c^2_{Al_2V_O}} = \exp\left(\frac{2E_{Al_2V_O}}{kT}\right)\sum_{i=1}^{3} x_i\exp\left(-\frac{E^{(i)}_{Al_4[V_O]_2}}{kT}\right),$$

$$c_i = \frac{N_i}{N_{lat}}, \tag{10}$$

where the energy parameters may now be read off from Table II. This formula, together with the requirement that all available Al ions are present in either Al_2V_O or $Al_4[V_O]_2$ states can then be used to determine the fraction of Al ions present in each kind of state at a given temperature and Al_2O_3 concentration. In Fig. 5(a) the results for temperatures

(a)

(b)

(c)

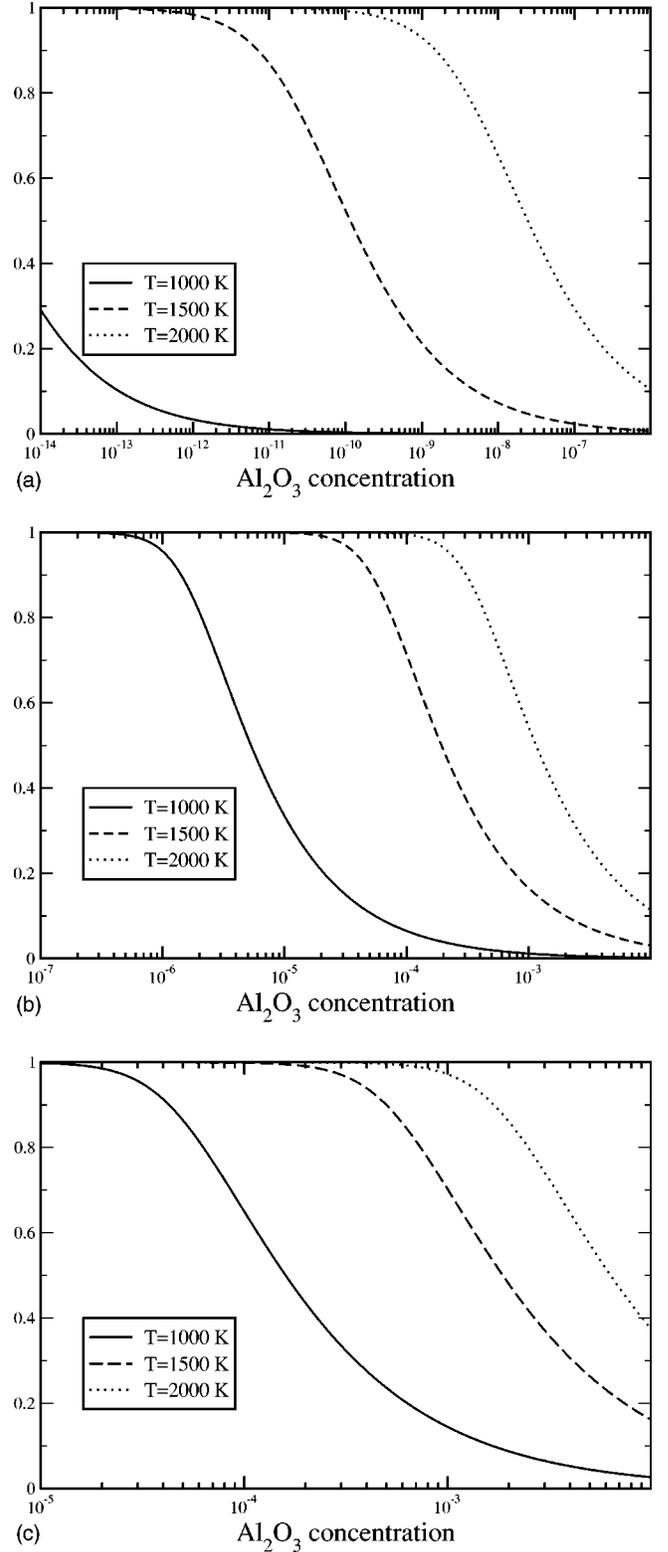FIG. 5. Fraction of Al ions in the Al_2V_O state as a function of Al_2O_3 concentration and temperature for various assumptions about Al_2V_O properties in the amorphous state of silica. (a) Al ions in the Al_2V_O state are paired. (b) Al ions in the Al_2V_O state move independently in the lattice. (c) Same as (b) with a lower energy estimate for the independent Al ions (see text for explanation).

of 1000, 1500, and 2000 K are plotted. It can be seen that the Al$_4$[V_O]$_2$ states are completely dominant for all Al$_2$O$_3$ concentrations of practical interest (natural quartz usually contains Al impurities in the ppm range), even at the highest temperatures. This seems to rule out the presence of Al$_2V_O$ units in α-quartz (which has actually transformed into β-quartz at these high temperatures), unless the crystal is far from thermodynamic equilibrium. On the other hand, the results do not necessarily imply the predominance of Al$_4$[V_O]$_2$ structures since states in which the O vacancy is separated from one or more of the Al ions have not been considered here. Although these states are likely to be still higher in energy they will be favored by entropy considerations at sufficiently low concentrations.

Since the two Al ions in the Al$_2V_O$ structure are only connected structurally (they share an O vacancy) one can speculate that they might be free to move away from each other in an amorphous silica host where the concept of an O vacancy is not so well defined. This is in contrast to the Al$_4$[V_O]$_2$ states, which are kept together by electrostatic forces as argued in Sec. II A. The simplest and most radical assumption is completely independent motion of the Al ions. In this case Eq. (10) is replaced by

$$\frac{c_{\text{Al}_4[V_O]_2}}{c_{Al}^4} = \exp\left(\frac{2E_{\text{Al}_2V_O}}{kT}\right)\sum_{i=1}^{3} x_i \exp\left(-\frac{E^{(i)}_{\text{Al}_4[V_O]_2}}{kT}\right),$$

(11)

c_{Al} being the concentration of isolated Al ions. The resulting fraction of Al ions in this state is plotted in Fig. 5(b) for the same temperatures as in Fig. 5(a). The splitting of the Al$_2V_O$ state is seen to greatly disfavor the formation of Al$_4$[V_O]$_2$ complexes, so that the independent Al ions are now expected to be dominant in the 10–100-ppm concentration range usually found in glass made from natural quartz samples. On the other hand, the Al$_4$[V_O]$_2$ state is still dominant for the high end of the concentration range investigated here, which is relevant for commercial Al-doped glass as used in, e.g., rare-earth doped optical amplifiers.

The results in Fig. 5(b) were obtained under the assumption that the independent Al ions still had the same mean energy as those in the α-quartz Al$_2V_O$ structure. However, one could argue that ions moving freely would preferably occupy positions in the lattice where they could form an extra Al-O bond. Taking the energy gain from the formation of a fourth Al-O bond to be 0.1 eV per Al atom as in the cristobalite host the curves of Fig. 5(b) are not changed very much. Taking the gain to be 0.44 eV as estimated from the comparison of α-quartz and α-cristobalite results one obtains the curves depicted in Fig. 5(c). The Al$_4$[V_O]$_2$ states are still dominant at the highest concentrations, but for doping in the 0.1–1 % range a mixture of states is present. As discussed above, the 0.44-eV energy gain is probably an overestimate due to the difference in size of the supercells used. On the other hand, in amorphous silica one could speculate that the energy gain would be site dependent and that certain favorable sites would be preferentially occupied, thus increasing the importance of the isolated Al state. However, obtaining a reliable estimate of such a site energy dis-

TABLE III. Hyperfine parameters (in cm^{-1}) for the paramagnetic states AlV_O and [Al$_2V_O$]$^-$. Only the isotropic coupling, A_{iso}, and the largest component of the anisotropic matrix, A_{an}, are given. Atom 1 is at the short-bonded site which is always three coordinated, while atom 2 is at the long-bonded site and may be three or four coordinated. The Al[3]-Al[4] structure is the equilibrium geometry of the neutral Al$_2V_O$ state. See text for further details.

System	Atom 1		Atom 2	
	A_{iso}	A_{an}	A_{iso}	A_{an}
Al[3]-Si[3]	0.0001	0.0000	−0.0418	−0.0047
Al[3]-Si[4]	0.0056	0.0002	−0.0085	−0.0002
Si[3]-Al[4]	−0.0446	−0.0046	−0.0001	0.0000
Al[3]-Al[3]	0.0141	0.0021	0.0134	0.0020
Al[3]-Al[4]	0.0315	0.0029	0.0008	0.0000

tribution is an extremely demanding computational problem beyond the scope of the present work.

C. Hyperfine parameters

Hyperfine parameters have been calculated for the various AlV_O states as well as for the [Al$_2V_O$]$^-$ state. For the latter, calculations were performed in two geometries: The equilibrium geometry of the neutral state in which the unpaired spin is found to be essentially localized on the Al[3] ion and the equilibrium geometry of the negative charge state, in which the unpaired electron forms a covalent bond between the two Al ions. The theoretical results are summarized in Table III. All hyperfine tensors are found to have approximate axial symmetry (to an accuracy of ~1%), except for that of the rebonded Al ion in the unrelaxed [Al$_2V_O$]$^-$ configuration, which is very small. This means that two components of the anisotropic part are identical, while the third is twice as large and has the opposite sign, so that the anisotropic tensor is traceless. In the table, only the largest component of the anisotropic term is therefore given.

Experimentally, most EPR studies of crystalline α-quartz have found signals corresponding to Al[4] ions, either in the neutral isolated state or in the presence of a positive alkali ion such as H, Li, Na, etc. The EPR signals are only seen upon irradiation of the samples. It is believed that the Al ions in the unirradiated material are present in substitutional positions in the quartz lattice, with an extra electron filling the hole in the valence band arising from the reduced valence of the Al ion compared to Si. An alkali ion is present nearby to compensate the excess charge. In natural quartz containing only trace amounts of Al there is often sufficient alkali impurities present to compensate all Al ions. In silica glass doped primarily with Al this is obviously not the case, and these states are therefore less interesting in this context. Brower measured another series of hyperfine signals in silica glass which he interpreted as coming from Al[3] ions with a trapped electron, either isolated or in the presence of an alkali ion.[13] The signal attributed to isolated Al[3] was found to have an isotropic hyperfine parameter of 0.0331 cm^{-1} and an anisotropic coupling of 0.0030 cm^{-1} (largest value of anisotropic matrix) in very good agreement with the theoretical

result for the unrelaxed $[Al_2V_O]^-$ state in which the unpaired spin is localized on a single Al[3] ion. On the other hand, no signal corresponding to the relaxed $[Al_2V_O]^-$ geometry was seen. The signal from Al[3] was not observed in crystalline α-quartz and was also absent in glasses containing high concentrations of alkali ions. The concentration of Al ions in the Al[3]-containing samples was 10–50 ppm by weight. This is below the concentration regime where the $Al_4[V_O]_2$ states would be expected to become important if the Al ions are uncorrelated, provided that the thermodynamical considerations of the previous section are applicable. On the other hand, if the Al ions are paired (as is necessarily the case in crystalline quartz, where they share an O vacancy) the $Al_4[V_O]_2$ state is expected to become dominant at much lower concentrations. The fact that Al[3] ions are seen in glass but not in quartz can thus be taken as an indication that Al ions are indeed uncorrelated in the amorphous state at low concentrations. The absence of an EPR signal corresponding to the relaxed $[Al_2V_O]^-$ configuration is another strong argument for this hypothesis.

Concerning the various AlV_O states it is interesting to notice that none of them give rise to a strong ^{27}Al hyperfine signal. Therefore the signal measured by Brower has no contribution from such structures. In the state with a rebonded Si atom all hyperfine parameters are quite small, indicating that the unpaired spin is largely located in the interstitial region. In the other states, the spin is almost completely localized on the Si cation. The hyperfine parameters found are slightly larger than the experimental results for the E'_1 center in pure silica, but in good agreement with the theoretical results of Boero et al.,[30] suggesting that the difference is related to the theoretical approximations rather than the presence of Al. Brower observed that the magnitude of the Si E'_1 signal appeared to follow the Al concentration, and speculated that this might be related to an AlV_O state.[13] The present calculations show that this is a valid hypothesis insofar as the hyperfine AlV_O signal should be similar to the ordinary Si-Si E'_1 signal.

D. Core level shifts

Various forms of core-level spectroscopies have been found to provide useful information about the chemical states of impurities in silica. In crystalline samples, x-ray fluorescence (XFS) from the K_α emission provides a clear distinction between different coordination states of cations such as Al, Si, and Ge. It has recently been shown that this quantity is predicted with very good accuracy by DFT calculations.[11] The calculated chemical shifts, referenced to metallic Al, are reported in Table IV for the Al ions in the Al_2V_O, $Al_4[V_O]_2^{(2)}$, and $Al_4[V_O]_2^{(3)}$ geometries. Generally, the shifts have been found to follow the coordination number of the Al ion in question quite closely, so that the interstitial Al[4] ion in the $Al_4[V_O]_2^{(2)}$ geometry has a shift similar to the substitutional ions. The shifts are, as is usually the case, found to increase with increasing coordination number. This can be understood as an effect of decreasing charge density at the Al cation: The $2p$ core hole provides a less attractive electrostatic potential for the valence electrons than the more compact $1s$ hole, meaning that the attraction between core hole and valence electrons will be stronger for the $1s$ hole, i.e., the initial state energy of the K_α transition is reduced more than the final-state energy by the interaction with the valence electrons. Therefore a smaller valence charge density on Al will lead to larger transition energies, i.e., a larger chemical shift. It is noteworthy that the shift of the Al[5] ion in $Al_4[V_O]_2^{(3)}$ is larger than the shift of Al[6] in crystalline Al_2O_3 (also given in Table IV). This shows that the Al ion becomes more positive in a silica environment, which is a reasonable finding given that the sp levels of Al are higher in energy than those of Si. Another interesting result is that the chemical shift of the rebonded Al ion in the Al_2V_O state is close to that of the substitutional ions in the $Al_4[V_O]_2$ states, indicating that the charge transfer away from the Al core region through the stretched bond is as effective as that which takes place through the bonds of the substitutional ions. The results presented so far show that the chemical shifts of the Al K_α line can provide a measure of the distribution of Al between different coordination states, but that it cannot distinguish ions of the same coordination in different structures (such as Al[4] in Al_2V_O and $Al_4[V_O]_2$). The situation is different if one considers the shifts of the $1s$ or $2p$ states individually. These shifts can be measured by x-ray photoemission spectroscopy (XPS). In Table V the relative

TABLE IV. Calculated chemical shifts of the Al K_α radiation line in different impurity states and in crystalline Al_2O_3.

System	Atom	Coordination	$K\alpha$ chem. shift (eV)
Al_2V_O	Al1	3	0.257
	Al2	4	0.339
$Al_4[V_O]_2^{(2)}$	Al1	4	0.340
	Al2	4	0.320
	Al3	4	0.336
	Al4	4	0.326
$Al_4[V_O]_2^{(3)}$	Al1	5	0.472
	Al2	4	0.345
	Al3	4	0.325
	Al4	4	0.328
α-Al_2O_3		6	0.434

TABLE V. Calculated chemical shifts of the Al $2p$ binding energy in the $Al_4[V_O]_2^{(2)}$ and $Al_4[V_O]_2^{(3)}$ structures.

System	Atom	Coordination	$\langle d_{Al-O} \rangle$ (Å)	E_{2p} (eV)
$Al_4[V_O]_2^{(2)}$	Al1	4	1.797	−2.07
	Al2	4	1.774	−0.52
	Al3	4	1.749	0.50
	Al4	4	1.759	0.02
$Al_4[V_O]_2^{(3)}$	Al1	5	1.907	−1.67
	Al2	4	1.762	−0.19
	Al3	4	1.766	−0.34
	Al4	4	1.756	0.53

shifts of the Al $2p$ levels in the Al$_4[V_O]_2^{(2)}$ and Al$_4[V_O]_2^{(3)}$ states are reported. Within each structure, the energies are measured relative to the mean level position of the substitutional Al ions (labeled Al[2]-Al[4] in Table V). The level positions of these ions in both case disperse over ~1 eV while the level position of the interstitial Al is 1.3–1.5 eV below the lowest substitutional $2p$ level. For the Al[4] ions the shifts correlate with the average Al-O bond lengths also given in Table V. These are again connected with the number of O[3] neighbor atoms since the bonds to these are longer. Thus the crucial difference between substitutional and interstitial Al atoms is the fact that the interstitials are only bonded to O[3] atoms, whereas the substitutionals typically have one or two O[3] neighbors.

The difference between XPS and XFS in distinguishing various Al species can be understood in the following way: When a core hole is introduced at an Al atom the valence of this atom is effectively changed by one, so extra charge is attracted from its O neighbors. The XPS shifts represent the difference in energy between core holes residing on different atoms and the energy gained by attracting extra charge from the neighbors depends on the nature of these (e.g., whether they are O[2] or O[3] species). However, these site differences largely cancel out when considering XFS shifts, which are differences between $1s$ and $2p$ core hole energies. The XFS shifts are roughly determined by the amount of charge present in the core region of the Al atom with the core hole, and this quantity appears to follow the coordination state of the atom quite closely. On the other hand, the energy gained by attracting the charge is higher if O[2] neighbors are present, which appears reasonable since the total charge on the O[3] species is lower as will be discussed further below.

Chemical shifts of the O $1s$ levels have been calculated in the Al$_4[V_O]_2^{(2)}$ and Al$_2V_O$ structures for O atoms in various coordination states. The $1s$ level position depends on the coordination number and nearest-neighbor species of the O atoms. The electronic charge on the O atom provides an attractive potential for the final-state $1s$ hole, so electron transfer to O will raise the $1s$ level position. The electronic charge on O is increased if Si neighbors are substituted by Al, since the Al valence orbitals are higher in energy than the Si ones, thus increasing the ionicity of the bond to O. On the other hand, an O[3] atom will carry a smaller electronic charge than an O[2], since a nonbonding O $2p$ electron is more localized on O than an electron bonding to Si or Al. Therefore O $1s$ core-level spectroscopy can in principle give information on the number of O[3] atoms, and also on the degree of Al correlation (by distinguishing O atoms bonded to more than one Al ion). In Table VI, the shifts of the $1s$ levels relative to that of a reference O atom in the same structure but far from the Al impurities are listed. Consider first the results for the Al$_2V_O$ geometry: In accordance with the above reasoning the O[2] atoms bonded to Al have their $1s$ levels shifted upwards. The O[3] atom has a negative shift of the $1s$ level, but comparison to the similar atom (neighbored by two Si and one Al) in the Al$_4[V_O]_2^{(2)}$ structure shows that the electron transfer to the core region of the O[3] atom becomes less efficient as the Al[4]-O[3] bond is

TABLE VI. Calculated chemical shifts of the O $1s$ level for some Al-bonded O atoms relative to a reference O in the same structure more than 5 Å from the Al impurities.

System	Atom	Neighbors	Chem. shift (eV)
Al$_2V_O$	1	Si,Al[3]	0.60
	2	Si,Al[4]	0.96
	3	Si,Al[4]	0.87
	4	2Si,Al[4]	−1.26
Al$_4[V_O]_2^{(2)}$	1	3Al	0.15
	2	Si,2Al	−1.14
	3	Si,2Al	−1.39
	4	2Si,Al	−2.04
	5	Si,Al	0.80
	6	Si,Al	0.90
	7	Si,Al	0.92
	8	Si,Al	1.40

stretched. This is in contrast to the result for the Al x-ray fluorescence data which indicated that the charge transfer away from the core region of the Al[4] atom is essentially the same in the two cases, implying that the stretched bond leaves more charge in the interstitial region between the nuclei.

The results obtained in the Al$_4[V_O]_2^{(2)}$ structure are also consistent with the simple arguments outlined above. The largest negative level shift is seen for the O[3] atom having only one Al neighbor. As the number of Al neighbors is raised, the chemical shift becomes less negative, and the $1s$ level of an O atom bonded to three Al atoms is close to that of the reference O atom far from the Al impurities. O[2] atoms with one Al neighbor have positive chemical shifts, as expected. Remarkably, one of these (atom 8) has a distinctly larger shift than the other three. The difference is most likely related to the fact that atom 8 has another Si-Al bonded O atom in its second neighbor shell, which is not the case for atoms 1 and 2. The presence of the nearby Al-O bond apparently pushes more negative charge onto atom 8, showing that the effect of an Al impurity on O $1s$ level shifts goes beyond the nearest-neighbor shell.

In summary, O $1s$ core-level shifts only provide a clear distinction between different chemical states of O atoms if an energy resolution better than ~1 eV can be achieved. Furthermore, for samples with low Al content, the signal from the Al-related O species will only be a small feature on the wings of the main Si-O-Si signal and may be difficult to detect.

E. Electric-field gradients

The electric-field gradient (EFG) at a particular nucleus is a traceless tensor given by

$$V_{ij} = \frac{\partial^2 V_e}{\partial x_i \partial x_j}, \tag{12}$$

where V_e is the electrostatic potential and the partial derivative is evaluated at the position of the nucleus in question. The tensor is conveniently expressed by two parameters, V_{zz} and η where V_{zz} is the principal component of largest magnitude and

$$\eta = \frac{|V_{xx} - V_{yy}|}{|V_{zz}|}, \quad |V_{zz}| \geqslant |V_{xx}| \geqslant |V_{yy}|. \quad (13)$$

The coupling of the electric-field gradient to the quadrupolar moment of a nucleus with nuclear spin quantum number $I > \frac{1}{2}$ can be measured in Mössbauer or NMR spectroscopy. The sign of V_{zz} is not experimentally accessible.

Theoretically, evaluation of the EFG tensor requires knowledge of the electrostatic potential at the nucleus in question, which in turn can be derived from the electronic density. Only the $l=2$ component of V_e (in an angular-momentum expansion centered on the nucleus) contributes. In the present formalism, the electronic density in the core region can be reconstructed as explained in Sec. II B, but it is important to notice that the EFG is a quantity which can be quite sensitive to the details of the calculation, and that several approximations are made in the present approach: First, the deformation (spherical as well as nonspherical) of the core states is neglected. Second, the valence basis orbitals in the core region are obtained in a free-atom calculation. Third, Vanderbilt's ultrasoft US-PP method, as well as Blöchl's PAW construction,[41] relies on a certain completeness assumption which is only approximately (although often with good accuracy) fulfilled. For these reasons, it is important to estimate the accuracy of the method by benchmarking it against other calculations using more accurate schemes.

The Al_2SiO_5 polymorphs silimanite and andalusite have recently been studied theoretically by several authors in order to extract EFG parameters for Al and O nuclei in various coordination states.[47,28,27] These studies were performed using the highly accurate full potential linear augmented plane-wave (FLAPW) method within the LDA approximation. The advantages of FLAPW compared to the present method is an explicit treatment of the wave function in the core region and the possibility of including semicore orbitals like the Al $2p$'s in the valence basis set. The existence of such accurate theoretical calculations as well as experimental data makes these crystals an obvious test case for the US-PP method. In Table VII EFG values for silimanite and andalusite obtained using US-PP's are compared to FLAPW results[27,28] as well as experimental values.[48,47] To investigate the importance of the atomic basis orbitals used in the US-PP construction, calculations were performed using two different O pseudopotentials denoted PP1 and PP2 in Table VII: PP1 is the one used for the structural relaxations, and has two atomic orbitals in each of the s and p channels. PP2 has an extra orbital in the p channel. It can be seen that the EFG values obtained with different FLAPW codes and parameter choices are generally in good agreement with each other although in a few cases deviations of 5–10% occur. The US-PP results for $|V_{zz}|$ at the Al nuclei are consistently smaller than those obtained using FLAPW, in one case by almost 40%, and are 20–50% smaller than the experimental values. On the other

TABLE VII. EFG parameters for the Al_2SiO_5 polymorphs silimanite and andalusite, reported in atomic units. The sign of V_{zz} has been omitted since it cannot be determined experimentally and was not given in Ref. 27. The signs reported in Ref. 28 were consistent with those obtained in the present work.

Atom		(Ref. 28)	(Ref. 27)	PP1	PP2	Expt.
Silimanite						
Al(1)	$|V_{zz}|$	0.239	0.238	0.232	0.231	0.271
	η	0.49		0.48	0.47	0.46
Al(2)	$|V_{zz}|$	0.187	0.189	0.137	0.137	0.206
	η	0.51		0.74	0.78	0.53
O(1)	$|V_{zz}|$	0.596	0.619	0.683	0.647	
	η	0.67		0.67	0.68	
O(2)	$|V_{zz}|$	0.525	0.537	0.622	0.583	
	η	0.01		0.05	0.07	
O(3)	$|V_{zz}|$	0.654	0.704	0.778	0.752	
	η	0.08		0.07	0.08	
O(4)	$|V_{zz}|$	0.669	0.733	0.827	0.775	
	η	0.52		0.47	0.49	
Andalusite						
Al(1)	$|V_{zz}|$	0.423	0.426	0.367	0.365	0.464
	η	0.08		0.14	0.14	0.10
Al(2)	$|V_{zz}|$	0.162	0.159	0.140	0.139	0.177
	η	0.73		0.93	0.95	0.67
O(1)	$|V_{zz}|$	0.473	0.489	0.560	0.535	
	η	0.18		0.15	0.14	
O(2)	$|V_{zz}|$	0.602	0.615	0.691	0.664	
	η	0.83		0.79	0.79	
O(3)	$|V_{zz}|$	0.409	0.420	0.478	0.463	
	η	0.85		0.88	0.87	
O(4)	$|V_{zz}|$	0.687	0.705	0.638	0.594	
	η	0.51		0.38	0.38	

hand, for all the O nuclei except one, $|V_{zz}|$ is overestimated compared to FLAPW (no experimental data exist here). However, the differences are somewhat smaller, around 10–15%. Most likely, the disagreement is caused by the frozen nature of the orbitals used in the PAW-like reconstruction of the charge distribution in the core region. When the Al ions are depleted of electronic charge by oxidation, the electronic orbitals must be expected to contract somewhat, increasing the asymmetric charge component close to the nucleus and thereby the EFG. The charge depleted from Al is transferred to the O ions, whose orbitals would therefore expand leading, by the same reasoning, to a reduction of the EFG. The atomiclike basis orbitals used in the US-PP construction are not able to respond to this charge redistribution, whereas the effect is included in the LAPW approximation. In the case of Al, an additional shortcoming of the US-PP method is that the deformation of the Al $2p$ states is not accounted for. This explains why the difference between LAPW and the US-PP method is larger for Al than for O. It can be seen from Table VII that the PP2 results for O are generally closer to the LAPW data, confirming that the limited variational degrees of freedom in the radial charge distribution is an important

TABLE VIII. EFG parameters for the Al ions in the Al$_2V_O$, Al$_4[V_O]_2^{(2)}$, and Al$_4[V_O]_2^{(3)}$ structures. The numbering is as in Table IV.

Atom	Z	$|V_{zz}|$ (a.u.)	η
Al$_2V_O$			
Al1	3	0.88	0.13
Al2	4	0.53	0.20
Al$_4[V_O]_2^{(2)}$			
Al1	4	0.36	0.98
Al2	4	0.48	0.77
Al3	4	0.25	0.31
Al4	4	0.45	0.29
Al$_4[V_O]_2^{(3)}$			
Al1	5	0.25	0.37
Al2	4	0.38	0.51
Al3	4	0.46	0.71
Al4	4	0.32	0.28

TABLE IX. EFG parameters for some of the O atoms bonded to Al in the Al$_4[V_O]_2^{(2)}$ structure. The reference atom is more than 5 Å away from any of the Al impurities.

Atom	Neighbors	$|V_{zz}|$ (a.u.)	η
1	3Al	0.54	0.35
2	Si,2Al	0.74	0.73
3	Si,2Al	0.65	0.81
4	2Si,Al	0.89	0.63
5	Si,Al	0.72	0.26
6	Si,Al	0.70	0.56
7	Si,Al	0.74	0.28
8	Si,Al	0.71	0.26
Ref.	2Si	1.02	0.17

source of error in the present calculations. For this reason, the PP2 potential was used for the calculation of EFG's in the SiO$_2$:Al$_2$O$_3$ structures.

The calculated EFG parameters for the Al ions in the Al$_2V_O$ and the two Al$_4[V_O]_2$ configurations of lowest energy are given in Table VIII. The Al[3] ion is found to have the highest $|V_{zz}|$ value and the Al[5] ion the lowest. However, the Al[4] ions show a large variation in the EFG strength, which can therefore not be taken as a measure of the coordination state alone. It is interesting to compare the results for doped quartz with those found for the Al$_2$SiO$_5$ crystals. In both andalusite and silimanite the ions denoted Al(1) are Al[6], while Al(2) are Al[5] (andalusite) or Al[4] (silimanite). Thus in this case the high-coordinated Al ions have the largest EFG's. The reason, at least for the case of silimanite, is likely to be the larger dispersion of Al-O bond lengths for the Al[6] species. Such a trend was not apparent in the Al$_4[V_O]_2$ structures. Therefore a shift of the Al ions towards higher coordination states in a glass should be accompanied by a decrease in EFG values.

EFG values for all O ions bonded to Al in the Al$_4[V_O]_2^{(2)}$ structure as well as a reference ion located far from the Al impurities are given in Table IX. The distribution of $|V_{zz}|$ values is more narrow here, and a clear distinction can be made between O ions with and without bonds to Al. On the other hand, considering the Al-bonded ions no clear distinction can be made between O[2] and O[3] species on the basis of the $|V_{zz}|$ values alone. However, as might be expected O[2] tends more towards axial symmetry ($\eta=0$) than O[3]. For the O[3] ions a trend towards higher EFG values with decreasing number of Al neighbors is apparent. These observations are consistent with the results obtained by Tossell and Cohen[27] in calculations using the Becke-Lee-Yang-Parr (LYP) functional on small clusters with a Gaussian basis set. The $|V_{zz}|$ values reported by these authors for O[3] species with various kinds of neighbors are close to or slightly higher than the present results, whereas their results for O[2] species with either two Si or one Si and one Al neighbor are

lower (by 10–20%) than the present findings. In view of the results for silimanite and andalusite, which showed that the US-PP method tends to overestimate O EFG values by ~10%, this indicates that the cluster models provide a good description of the O[2] species but overestimates the $|V_{zz}|$ values of O[3] atoms.

Experimentally, Al EFG parameters have only been studied in glasses with rather high Al$_2$O$_3$ concentrations (10 mole % or more) due to the limited sensitivity of NMR. The results recently reported by Schaller and Stebbins[17] for La- and Y-codoped aluminosilicates correspond to $|V_{zz}|$ values around 0.10–0.15 a.u. Similar values were obtained by Mc-Manus *et al.* for glass approximately of Mullite composition (3Al$_2$O$_3$:2SiO$_2$).[19] These values are considerably lower than the ones obtained here, which is remarkable given that the findings for the Al$_2$SiO$_5$ polymorphs suggest that the Al EFG values are somewhat underestimated by the US-PP method. This shows that Al in these materials sits in more symmetric local environments than the Al ions in the impurity structures studied here. Whether this is due to the greater flexibility of amorphous silica networks compared to the quartz supercells used here, or to the formation of more extended Si-Al-O structures at high Al$_2$O$_3$ concentrations, remains an open question. However, the comparison of structural data with the EXAFS results of Sen[14] discussed in Sec. III A suggests that the present approach does indeed overestimate the Al-O bond length dispersion slightly (Sen's experiments were conducted on glasses with an Al$_2$O$_3$ concentration below 1 mole %), and can therefore also be expected to overestimate the magnitude of the EFG tensors.

NMR spectroscopy on O ions is a difficult task due to the low abundance of the NMR-active ^{17}O isotope. Results for ^{17}O-enriched samples of sodium aluminosilicate glasses have been reported by several authors.[49–52] As an example, Dirken *et al.*[49] attributed $|V_{zz}|$ values of 0.87 and 0.60 a.u. in a NaAlSi$_3$O$_8$ glass to Si-O-Si and Al-O-Si linkages, respectively, in reasonable agreement with the results found here considering the tendency of the US-PP method to overestimate O EFG's. Interestingly, no evidence was found of Al-O-Al linkages, which are also absent in all the structures found in the present work. The absence of such links does not necessarily rule out Al clustering as seen from the present calculations where all Al ions have at least one Al in

the second neighbor shell, although no Al-O-Al links are found (disregarding O[3] species). Rather it demonstrates that certain Al structures avoiding Al-O-Al links are preferred.

IV. DISCUSSION

The structural and energetic results presented in the previous section suggest the following picture of Al_2O_3 impurity behavior in silica glass: At low concentrations Al will be present as isolated or paired Al[3] or Al[4] species depending on the local environment. As the Al_2O_3 concentration increases formation of $Al_4[V_O]_2$ states will gradually be favored. However, the results of Sec. III B show that the total energies obtained here cannot provide a quantitative estimate of the concentration range in which the transition to $Al_4[V_O]_2$ states occur. There are at least four difficult points:

(i) There is a large number of possible $Al_4[V_O]_2$ structures, even in an ordered host like α-quartz. Only a subset of these have been included in the present model.

(ii) It is not clear whether neutral, nonmagnetic Al impurities can move independently in amorphous silica, or whether they need to pair in order to share an O vacancy (as they must in a crystalline host). Both hypotheses were investigated in Sec. III B and were found to give quite different results for the impurity state distribution as a function of concentration.

(iii) The structural results for the Al_2V_O defect in α-quartz and α-cristobalite suggest that isolated Al impurities will have three strong bonds and one which is weaker or wholly absent. However, one could speculate that the greater relaxational freedom in silica glass (and, in particular, in a silica melt) would make the formation of Al[4] species with four strong bonds easier. If so, it is possible that the formation of $Al_4[V_O]_2$ species would not occur at all but the glass would consist of independent Al[4] ions up to very high Al_2O_3 concentrations.

(iv) Finally the assumption of a thermodynamical equilibrium state used in Sec. III B is questionable. It appears reasonable in melt-quenched glasses but may not be appropriate in other cases (e.g., glass manufactured by the sol-gel or plasma-enhanced chemical-vapor deposition (PECVD) methods).

Since the theoretical results does not provide a full understanding of Al impurity behavior it is important to consider the available experimental information. In the low-concentration regime, an important series of EPR experiments were carried out by Brower.[12,13] His assignment of a ^{27}Al hyperfine signal with an isotropic coupling constant of 0.0331 cm^{-1} to an Al[3] ion with a trapped electron is confirmed by the results of Sec. III C. There are several interesting aspects of Brower's results: First, he observed the Al[3] signal in silica manufactured from natural quartz by electrical melting in a vacuum or inert gas, but failed to observe it in similar quartz samples prior to melting. Second, he did not observe a signal corresponding to the one calculated in Sec. III C for a spin evenly distributed over two Al nuclei. And third, the concentration of paramagnetic Al[3] impurities was found to be $\sim 3 \times 10^{16}$ cm^{-3} after irradiation, and three

times higher after H sweeping. The first and second finding has implications for the question of Al pairing. In α-quartz, the equilibrium geometry of the Al_2V_O state had one Al[3] and one Al[4] atom with no chemical bonding between them. However, upon electron addition the weak Al-O bond of the Al[4] atom is broken and an Al-Al bond is formed. If the Al impurities in Brower's samples were present in Al_2V_O-like pairs one would expect at least some of them to form an Al-Al bonded state upon trapping an electron. Therefore the absence of the corresponding EPR signal is an indication that the Al ions are, in fact, not paired to each other. This could also explain why neither the Al[3] signal, nor the signal from the $[Al_2V_O]^-$ equilibrium geometry was observed in quartz samples. In crystalline quartz, neutral diamagnetic Al impurities have to be paired in order to share an O vacancy. The results presented in Fig. 5(a) show that the Al_2V_O state in this situation is disfavored for all concentrations of practical interest (the Al concentration in Brower's samples was 10–50 ppm by weight). However, if the Al ions in the Al_2V_O state become independent the state is stabilized up to an Al_2O_3 concentration range of $\sim 10^{-4}$–10^{-3} mole %, in agreement with Brower's observations for amorphous silica.

The concentration results reported by Brower are also significant. They put a lower limit of 1–3% on the fraction of Al ions in the Al[3] state. This suggests that many of the isolated Al ions in the glass do not form four strong bonds but rather that a distribution of bond lengths is present, i.e., that the notion of a site energy distribution for isolated Al ions suggested at the end of Sec. III B is not unreasonable. As long as $Al_4[V_O]_2$ states do not come into play one would expect the ratio between Al[3] and Al[4] ions to be more or less independent of concentration, and characteristic of the glass fabrication process. However, in a glass sample doped with 1.04% Al_2O_3 Brower did not report the Al[3] EPR signal.[13] This suggests that the Al[3] states at this high Al concentration were eliminated by the formation of $Al_4[V_O]_2$ structures.

An EXAFS study of Al in melt-quenched silica glass was recently undertaken by Sen.[14] The glass was doped with 7300 ppm Al_2O_3 by weight, corresponding to about 0.43 mole %. The EXAFS results for the local environment of Al, and their comparison to the equilibrium geometries found in the present work was discussed in Sec. III A. It was found that the average bond length, bond-length dispersions, and coordination numbers in the $Al_4[V_O]_2$ geometries were all in fair agreement with the experimental results. This is not the case for the Al_2V_O structure, where the bond-length dispersion due to the stretched fourth bond of the Al[4] ion becomes very large. Therefore Sen's results indicate that all but the most symmetric isolated Al ions (i.e., those having four strong bonds) have been eliminated in favor of $Al_4[V_O]_2$ states at the Al_2O_3 concentration of 0.4 mole %. Although this cannot be taken as a definite proof of $Al_4[V_O]_2$ dominance, comparison with Brower's results showing a significant Al[3] population at an Al concentration two orders of magnitude lower strongly suggests that a transition from isolated Al to $Al_4[V_O]_2$ structures takes place in between these two concentrations. Of course, this conclusion would be somewhat stronger if the EXAFS and EPR measurements had been performed on the same samples.

Numerous ^{27}Al NMR studies have been made on glasses with Al$_2$O$_3$ concentrations higher than 1 mole %. As discussed in Sec. III E, the quadrupole coupling constants contain only limited information on the local Al structure. The chemical shift tensor is thought to give a more reliable indication of the different Al coordination states. In glasses with Al$_2$O$_3$ concentrations at or below 10 mole %, peaks at $\sim$0, 30, and 60 ppm have been identified.[15,53,18] The peaks at 0 and 60 ppm are commonly assigned to Al[6] and Al[4], respectively. The peak around 30 ppm is in some cases assigned to Al[5],[54] in others to Al[4] in a distorted environment.[53] Somewhat mixed results regarding the concentration dependence of the peak intensities have been reported. Jin *et al.* studied sol-gel manufactured silica codoped with Al$_2$O$_3$ and 1 mole % Sm$_2$O$_3$ and found mainly NMR signals from α-Al$_2$O$_3$ crystallites at an Al$_2$O$_3$ concentration of 1 mole %.[18] However, at 10 mole % Al$_2$O$_3$ signals from Al[4] and Al[6] dissolved in the glass matrix were seen. Fujiyama *et al.*, using a different sol-gel process, reported an NMR spectrum with a clear Al[4] peak at 3 mole % Al$_2$O$_3$ concentration in the dried gel.[15] These results indicate that the Al states in sol-gel glasses are strongly dependent on the fabrication method, and are not adequately described by the thermodynamic considerations used here. In a recent study by Schmücker *et al.* of rapidly solidified aluminosilicate melts (10 mole % Al$_2$O$_3$) a broad NMR signal with a peak around 30 ppm and noticeable shoulders at 54 and 4 ppm was reported.[53] If the 30-ppm signal is interpreted as arising from Al[5] this finding is strongly at variance with the results presented here, as they would then imply that the majority of the Al impurities would be in the Al[5] state. On the other hand, if the peak is caused by distorted Al[4] tetrahedra, the Al$_4$[V_O]$_2$ structure remains a valid hypothesis. That this is the case is supported by the broad nature of the NMR signal, which suggests that a gradual variation of the chemical shift can be caused by distortion. Addition of Na$_2$O to the melts was found to increase and sharpen the peak around 54 ppm. Na$_2$O addition would be expected to lead to the formation of isolated Al[4] species compensated by Na$^+$ ions. Such Al impurities would have more symmetric tetrahedral environments than the Al ions in the Al$_4$[V_O]$_2$ structures,[55] and would therefore be expected to give a clearer Al[4] NMR signal.

In summary, an analysis of theoretical and experimental results regarding Al$_2$O$_3$-doped silica glasses suggest that formation of Al$_4$[V_O]$_2$ structures takes place somewhere in the concentration range between $\sim$0.01 and 1 mole %. To test this hypothesis theoretically, realistic simulations of Al impurity behavior in a random silica network are needed. This will involve quenches of supercells with hundreds or even thousands of atoms using realistic energy functionals such as those based on DFT, or tight-binding approximations to DFT. Presently, this appears a tall (but not completely unfeasible) order. On the experimental side, more systematic studies of Al$_2$O$_3$-doped silica in the range of low and intermediate concentrations would be needed. As is evident from the above discussion, it is important that a multitude of experimental techniques is employed simultaneously.

V. CONCLUSIONS

Two simple geometries for Al$_2$O$_3$ impurity units in SiO$_2$ have been investigated by DFT calculations in an α-quartz host. Al$_2$O$_3$ was assumed to exist either as two Si-substitutional Al impurities sharing an O vacancy (Al$_2V_O$), or as three substitutional Al ions in close proximity compensated by a fourth Al impurity in the interstitial region of the silica network (Al$_4$[V_O]$_2$). The latter configuration was found to be energetically favored by about 1.4 eV per Al$_2$O$_3$ unit, and simple thermodynamic estimates indicate that these states will be dominant at least for Al$_2$O$_3$ concentrations above 0.1–1 mole %. Various experimental signatures of the above-mentioned states, as well as that of a single neutral substitutional Al atom at an O vacancy (AlV_O) have been calculated. The hyperfine tensor calculated for the Al$_2V_O$ state with a trapped electron in a geometry with one Al[3] and one Al[4] ion was in good agreement with a signal observed by Brower in amorphous silica.[12,13] However, this geometry was destabilized by the electron addition and the hyperfine tensors for the equilibrium geometry did not correspond to experimentally observed signals, suggesting that Al[3] ions in amorphous silica are not paired. The ^{27}Al hyperfine tensors were found to be very small in the AlV_O states, whereas the ^{29}Si tensors were close to those found at positively charged O vacancies in pure silica. Core-level chemical shifts were calculated for Al and O ions in various coordination states. It was found that shifts of the Al K_α flourescence line provided a measure of Al coordination, whereas the $1s$ and $2p$ level positions by themselves were more sensitive to whether the Al ion was substitutional or interstitial in the silica network. The O $1s$ chemical shifts were found to be sensitive to coordination as well as the number of Al neighbors to the O ion. EFG parameters were evaluated for Al ions and their O neighbors, but were found to have a complicated dependence on the nature of the local environment, thus precluding the prospect of using these parameters as a measure of, e.g., the coordination state of the ions.

---

[1] S. Sen and J. Stebbins, J. Non-Cryst. Solids **188**, 54 (1995).

[2] E. Delevaque, T. Georges, M. Monerie, P. Lomouler, and J. F. Bayon, IEEE Photonics Technol. Lett. **5**, 73 (1993).

[3] R. H. D. Nuttall and J. A. Weil, Can. J. Phys. **59**, 1696 (1981).

[4] R. H. D. Nuttall and J. A. Weil, Can. J. Phys. **59**, 1709 (1981).

[5] R. H. D. Nuttall and J. A. Weil, Can. J. Phys. **59**, 1886 (1981).

[6] R. S. Dickson and J. A. Weil, Can. J. Phys. **68**, 630 (1990).

[7] D. F. Howarth, M. J. Mombourquette, and J. A. Weil, Can. J. Phys. **75**, 99 (1997).

[8] K. Fukumi, A. Chayahara, M. Makihara, K. Fujii, J. Hayakawa, and M. Satou, J. Am. Ceram. Soc. **77**, 3019 (1994).

[9] K. Fukumi, A. Chayahara, N. Kitamura, J. Nishii, K. Kadono, M.

Makihara, K. Fujii, and J. Hayakawa, J. Appl. Phys. **79**, 1060 (1996).

[10] J. Laegsgaard and K. Stokbro, Phys. Rev. B **61**, 12 590 (2000).

[11] J. Laegsgaard, Phys. Rev. B **63**, 193102 (2001).

[12] K. L. Brower, Phys. Rev. Lett. **41**, 879 (1978).

[13] K. L. Brower, Phys. Rev. B **20**, 1799 (1979).

[14] S. Sen, J. Non-Cryst. Solids **261**, 226 (2000).

[15] T. Fujiyama, T. Yokoyama, M. Hori, and M. Sasaki, J. Non-Cryst. Solids **135**, 198 (1991).

[16] M. Schmücker, H. Schneider, and K. J. D. MacKenzie, J. Non-Cryst. Solids **226**, 99 (1998).

[17] T. Schaller and J. F. Stebbins, J. Phys. Chem. B **102**, 10 690 (1998).

[18] J. Jin, S. Sakida, T. Yoko, and M. Nogami, J. Non-Cryst. Solids **262**, 183 (2000).

[19] J. McManus, S. E. Ashbrook, K. J. D. MacKenzie, and S. Wimperis, J. Non-Cryst. Solids **282**, 278 (2001).

[20] M. J. Mombourquette, J. A. Weil, and P. G. Mezey, Can. J. Phys. **62**, 21 (1984).

[21] M. J. Mombourquette and J. A. Weil, Can. J. Phys. **63**, 1282 (1985).

[22] F. Sim, C. R. A. Catlow, M. Dupuis, and J. Watts, J. Chem. Phys. **95**, 4215 (1991).

[23] A. Continenza and A. DiPomponio, Phys. Rev. B **54**, 13 687 (1996).

[24] M. Magagnini, P. Giannozzi, and A. DalCorso, Phys. Rev. B **61**, 2621 (2000).

[25] G. Pacchioni, F. Frigoli, D. Ricci, and J. A. Weil, Phys. Rev. B **63**, 054102 (2001).

[26] J. Laegsgaard and K. Stokbro, Phys. Rev. Lett. **86**, 2834 (2001).

[27] J. A. Tossell and R. E. Cohen, J. Non-Cryst. Solids **286**, 187 (2001).

[28] M. Iglesias, K. Schwarz, P. Blaha, and D. Baldomir, Phys. Chem. Miner. **28**, 67 (2001).

[29] E. D. Lacy, Phys. Chem. Glasses **4**, 234 (1963).

[30] M. Boero, A. Pasquarello, J. Sarnthein, and R. Car, Phys. Rev. Lett. **78**, 887 (1997).

[31] G. Lucovsky, A. Rozaj-Brvar, and R. F. Davis, in *The Structure of Non-Crystalline Materials*, edited by P. H. Gaskell, J. M. Parker,

and E. A. Davis (Taylor and Francis, London, 1982), pp. 193–205.

[32] T. D. Taylor and G. E. Rindone, J. Am. Ceram. Soc. **53**, 692 (1970).

[33] G. Engelhardt, M. Nofz, K. Forkel, F. G. Wihsmann, M. Mägi, A. Samoson, and E. Lippmaa, Phys. Chem. Glasses **26**, 157 (1985).

[34] K. F. Young and H. P. R. Frederikse, J. Phys. Chem. Ref. Data **2**, 313 (1973).

[35] P. Hohenberg and W. Kohn, Phys. Rev. **136**, B864 (1964).

[36] W. Kohn and L. Sham, Phys. Rev. **140**, A1133 (1965).

[37] J. P. Perdew, J. A. Chevary, S. H. Vosko, K. A. Jackson, M. R. Pederson, D. J. Singh, and C. Fiolhais, Phys. Rev. B **46**, 6671 (1992).

[38] D. Vanderbilt, Phys. Rev. B **41**, 7892 (1990).

[39] K. Laasonen, A. Pasquarello, R. Car, C. Lee, and D. Vanderbilt, Phys. Rev. B **47**, 10 142 (1993).

[40] J. Laegsgaard and K. Stokbro, Phys. Rev. B **63**, 075108 (2001).

[41] P. E. Blöchl, Phys. Rev. B **50**, 17 953 (1994).

[42] G. Kresse and D. Joubert, Phys. Rev. B **59**, 1758 (1999).

[43] C. G. VandeWalle and P. E. Blöchl, Phys. Rev. B **47**, 4244 (1993).

[44] H. M. Petrilli, P. E. Blöchl, P. Blaha, and K. Schwarz, Phys. Rev. B **57**, 14 690 (1998).

[45] P. E. Blöchl, Phys. Rev. B **62**, 6158 (2000).

[46] G. Pacchioni, G. Ieranò, and A. M. Marquez, Phys. Rev. Lett. **81**, 377 (1998).

[47] P. L. Bryant, C. R. Hartwell, K. Wu, F. R. Fronczek, R. W. Hall, and L. G. Butler, J. Phys. Chem. A **103**, 5246 (1999).

[48] M. Raymond, Phys. Rev. B **3**, 3692 (1971).

[49] P. J. Dirken, S. C. Kohn, M. E. Smith, and E. R. H. Vaneck, Chem. Phys. Lett. **266**, 568 (1997).

[50] Z. Xu, H. Maekawa, J. V. Oglesby, and J. F. Stebbins, J. Am. Ceram. Soc. **120**, 9894 (1998).

[51] J. F. Stebbins, S. K. Lee, and J. V. Oglesby, Am. Mineral. **84**, 983 (1999).

[52] S. K. Lee and J. F. Stebbins, J. Non-Cryst. Solids **270**, 260 (2000).

[53] M. Schmücker, K. J. D. MacKenzie, H. Schneider, and R. Meinhold, J. Non-Cryst. Solids **217**, 99 (1997).

[54] J. T. Kohli, J. E. Shelby, and J. S. Frye, Phys. Chem. Glasses **33**, 73 (1991).

[55] M. Magagnini, Phys. Rev. B **62**, 1524 (2000).